

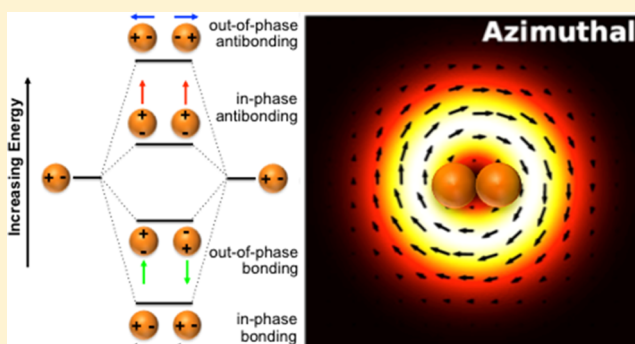
Dark Plasmon Modes in Symmetric Gold Nanoparticle Dimers Illuminated by Focused Cylindrical Vector Beams

Tian-Song Deng,^{†,‡,||} John Parker,^{‡,§,||} Yuval Yifat,^{‡,||} Nolan Shepherd,^{†,‡} and Norbert F. Scherer^{*,†,‡}[†]The James Franck Institute, [‡]Department of Chemistry, [§]Department of Physics, University of Chicago, Chicago, Illinois 60637, United States

Supporting Information

ABSTRACT: The plasmon hybridization model of electromagnetic coupling between plasmonic nanoparticles predicts the formation of lower energy “bonding” and higher energy “antibonding” modes in analogy with the quantum mechanical description of chemical bonding. For a symmetric metallic nanoparticle dimer excited by linearly polarized light, the hybridization picture predicts that in-phase coupling of the dipole moments is optically allowed, creating bright “modes”, whereas the out-of-phase coupling is dark due to the cancellation of the oppositely oriented dipole moments (in the quasistatic approximation). These bright modes are electric dipolar in nature and readily couple to scalar (i.e., linearly or circularly polarized) beams of light. We show that

focused cylindrical vector beams, specifically azimuthally and radially polarized beams, directly excite dark plasmon modes in symmetric gold nanoparticle (AuNP) dimers at normal incidence. We use single-particle spectroscopy and electrodynamic simulations to study the resonance scattering of AuNP dimers illuminated by azimuthally and radially polarized light. The electric field distributions of the focused azimuthal or radial beams are locally polarized perpendicular or parallel to the AuNP dimer axis, but with opposite directions at each particle. Therefore, the associated combinations of single-particle dipole moments are out-of-phase, and the excitation (resonance) is of so-called “dark modes”. In addition, multipole expansion of the fields associated with each scattering spectrum shows that the vector beam excitation involves driving multipolar, e.g., magnetic dipolar and electric quadrupolar, modes, and that they even dominate the scattering spectra (vs electric dipole). This work opens new opportunities for investigating dark plasmon modes in nanostructures, which are difficult to selectively excite by conventional polarized light.



INTRODUCTION

Noble-metal nanoparticles (NPs) can support localized surface plasmon resonances (LSPRs), the collective coherent oscillations of conduction electrons in metal nanocrystals that exhibit strong far-field scattering and near-field enhancement of the excitation field.¹ In individual metallic nanoparticles, the LSPR depends on the size and shape of the nanoparticle and the dielectric environment.² When two or more NPs are placed in close proximity to each other, LSPRs are not the most appropriate basis or description of the resonance due to the strong near-field coupling of the LSPRs of the individual particles.³ The electrodynamic coupling of nanoparticle plasmons can lead to large spectral shifts, enormous electric field enhancement in the gap regions, as well as a new set of plasmonic modes. These features of coupled metal nanoparticles (nanocrystals) enable various applications in plasmon-enhanced spectroscopy and nano-optics, including plasmon rulers,^{4–6} sensing,⁷ surface-enhanced Raman spectroscopy,^{8–10} fluorescence,¹¹ upconversion,¹² optical switches,¹³ plasmonic circular dichroism,¹⁴ nanometric optical tweezers,¹⁵ and metallic

nanoscale lenses.¹⁶ Thus, the fundamental properties of coupled plasmons have been translated to many applications.

The plasmon hybridization model developed by Halas and Nordlander et al.^{17,18} has been applied to explain the optical properties of various electrodynamically coupled plasmonic nanostructures. In this model, the plasmon modes of a coupled nanostructure are expressed in terms of interactions between the individual component resonances. The hybridized plasmon states are analogous to the formation of molecular orbitals from the hybridization of individual atomic wave functions used to describe chemical bonding.¹⁸ For example, for a metal nanoparticle dimer with individual states, φ_1 and φ_2 , the hybridized plasmon states can be either in-phase ($\varphi_1 + \varphi_2$, enhancing dipole moment) or out-of-phase ($\varphi_1 - \varphi_2$, vanishing dipole moment) coupling, corresponding to spectrally broad super-radiant (bright) or narrow subradiant (dark) plasmon spectroscopic “modes”. In the case of a symmetric dimer

Received: October 25, 2018

Revised: October 31, 2018

Published: November 26, 2018

illuminated by linearly polarized (LP) light, the in-phase coupling of the individual dipole moments is optically allowed, whereas the out-of-phase mode is spectrally dark due to the cancellation of the equal, but oppositely oriented dipole moments of the two particles.¹⁸ These bright plasmon modes have been extensively studied, since they can be simply excited by conventional LP light. However, dark plasmons offer opportunities for enhanced plasmonic applications. Due to its vanishing dipole moment, the reradiation of energy of dark plasmons in the far-field is significantly smaller than that of the bright plasmons, resulting in much stronger near-field enhancement. Therefore, dark resonances present higher-quality factors due to smaller radiative damping, and the interference between spectrally overlapping narrow dark modes and broad bright modes leads to plasmonic Fano resonances.

One way to generate dark modes is to break the symmetry of a nanostructure. For instance, dark modes have been observed in heterodimers,^{10,19–21} gold nanorod dimers,^{22–24} gold bipyramid dimers,²⁵ and asymmetric core–shell particles.²⁶ In these nanostructures, out-of-phase coupling is allowed due to a broken exchange symmetry of the unequal dipole moments of the individual particles. A second approach is nonoptical excitation by electron beams, which can excite and probe dark modes in symmetric nanostructures with electron energy-loss spectroscopy.^{27,28} A third approach for excitation of dark plasmons employs tailored illumination techniques, such as localized (near-field) emitters²⁹ or far-field excitation by non-normal incidence (retardation effects),³⁰ spatial phase shaping,³⁰ and cylindrical vector beams (CVBs).³¹ Cylindrical vector beams, in particular azimuthally polarized (AP) and radially polarized (RP) beams, allow the selective excitation of multipolar plasmon modes in nanostructures^{32,33} and have been used for improving the optical resolution in light microscopy³⁴ and nonlinear microscopy of nanostructures.³⁵ The response of plasmonic clusters excited by CVBs allows efficient excitation of dark modes in symmetric clusters of metallic nanoparticles.^{33,36} In addition, CVBs enable the excitation of Fano-like resonances in highly symmetric plasmonic clusters (e.g., trimer and quadrumer), a result of the coupling of broad bright modes and narrow dark modes of different multipolar orders sharing similar charge distributions.³⁶ Therefore, CVBs are ideal far-field illumination sources to excite dark plasmon modes in symmetric metallic nanoparticle clusters.

Despite this potential, most of the reported work using CVBs involved dielectric particles (e.g., Si)^{37–39} and lithographically patterned nanostructures.^{40–42} Moreover, the polycrystalline quality of the metallic particles made by lithography results in greater damping and concomitantly weaker plasmon coupling. In addition, the precision of lithography is limited to the scale of ~ 10 nm making it difficult to study the gaps at the 1 nm level, which should have strong plasmon coupling and hybridization. Published work is limited to near-field scanning optical microscopy⁴¹ or only radial beam illumination⁴⁰ without theoretical simulations for interpretation. Thus, lithographically patterned nanostructures are not ideal for direct experimental validation of the hybridization model.

In this paper, we report experimentally measured scattering spectra of symmetric gold nanoparticle (AuNP) dimers illuminated by CVBs, and finite-difference time-domain (FDTD) electrodynamic simulations performed to analyze the plasmon modes for various interparticle separations and coupling. Moreover, using the novel multipole expansion

method we developed,³³ we show that new multipolar (e.g., electric quadrupole (eQ) and/or magnetic dipole (mD)) modes that cannot be excited by linearly polarized light are excited by RP and AP beams. This work is the first experimental measurement of plasmonic dark mode excitation in symmetric metallic nanoparticle dimers using CVB illumination.

METHODS

Preparation of AuNPs with Different Silica Shell Thickness. The AuNP@SiO₂ particles were purchased from nanoComposix, with ~ 20 nm silica shell thickness. To get smaller gap distances, we etched a portion of silica shell using ammonia. Specifically, 20 μ L of the AuNP@SiO₂ solution was added to 2 mL of H₂O, followed by addition of 20 μ L of ammonia (28–30%, Sigma-Aldrich). After gently shaking for a few seconds, the solution was left undisturbed for 12 h. The solution was centrifuged, the supernatant removed, and the pellet was redispersed in water for three cycles. After etching, the silica shell thickness decreased to ~ 15 nm. To get larger gap distances, we grew a new layer of silica on the original AuNP@SiO₂ particles.⁴³ To do this, 20 μ L of AuNP@SiO₂ solution was added to 2 mL of methanol, then 0.2 mL of water and 0.2 mL of ammonia were added while stirring, followed by two additions of 40 μ L of tetraethyl orthosilicate solution (20 vol % in methanol) at 2 h intervals. The reaction was allowed to continue while stirring for 24 h, resulting in a silica shell thickness of ~ 45 nm. The resulting particles were washed with water three times and dispersed in water for further use.

Measurements of Scattering Spectra of AuNP Dimers. The scattering spectra were measured using a home-built microscopy setup. A schematic of the vector beam spectroscopy setup is shown in Figure 1a. A spatially coherent (broadband) white light continuum (Fianium, White Lase SC400, emitting between 500 and 1200 nm) was coupled to an inverted optical microscope equipped with an oil immersion objective with numerical aperture, NA ≤ 1.4 (Olympus, IX-81; SAPO 100X). The vector beam generator was placed outside of the microscope, just behind the linear polarizer and positioned using a translation stage for fine adjustment. The vector beam generator used here is a liquid-crystal-based polarization converter (ARCOptix, Switzerland), which can generate azimuthally and radially polarized cylindrical vector beams.⁴⁴ The back-scattered images and spectra of the sample plane were recorded either by a scientific complementary metal-oxide-semiconductor (sCMOS) array detector (Andor, Neo) connected to the eye piece of the microscope or by a charge coupled device (CCD, Andor, Newton) connected to an imaging spectrometer (Shamrock 193i) coupled to the side port of the microscope. The halogen light source on the top is coupled to an optical fiber to illuminate the samples. The aqueous dispersion of nanoparticles was drop-casted on a formvar-coated transmission electron microscope (TEM) finder grid and dried overnight.

We conducted correlated single-particle spectroscopy and structure measurements of specific dimers. Before taking scattering spectra, TEM images were acquired with a Tecnai 30F TEM (FEI) with a 300 kV accelerating voltage. The grid was then placed on a glass cover slide. Subsequently, immersion oil ($n = 1.51$) was put on top of the grid to match the index of the glass slide and reduce the scattering of the silica ($n = 1.45$) when AuNP@SiO₂ was used. Finally, the sample cell was closed with another cover slide on the top, forming a sandwiched structure, with the grid (embedded in immersion oil) between two glass

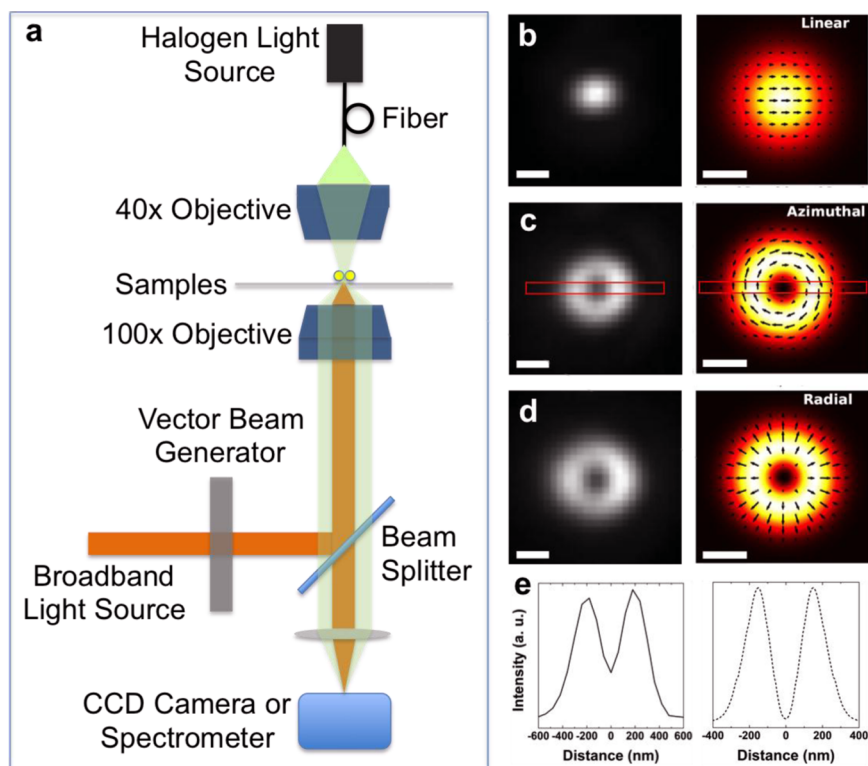


Figure 1. Setup for single-particle spectroscopy with vector beams' illumination and beam profiles. (a) Setup for single-particle spectroscopy with optical vector beams. Note that not all lenses and optical components are shown for simplicity. (b–d) Optical microscopy images (left column) and intensity profiles (right column) of linear, azimuthal, and radial polarized beams. The arrows in the intensity profiles indicate the instantaneous electric field polarization. (e) Intensity profiles of experimental (left) and simulated (right) optical beams within the red rectangular areas of the azimuthal beams shown in (c). All scale bars in (b)–(d) are 200 nm. Note that the simulated beams expand from the source plane.

slides. Figure S1 shows images of the same area of the grid taken by TEM and optical microscopy demonstrating that we can obtain the structure and spectra of the identical dimers. Note that the dimers chosen for measurements are well separated from other nanoparticles ($\sim 5 \mu\text{m}$) to avoid scattering from neighboring particles that could affect the measurements.

Simulations of AuNP Dimer Structures. Simulations of the Au nanoparticle dimer were performed using the FDTD method⁴⁵ via a freely available software package (MEEP).⁴⁶ Au nanoparticle dimers were placed in an oil environment (index 1.50) with gaps obtained from TEM images. The dielectric function of Au was obtained by fitting the Drude–Lorentz model to fit the Johnson–Christy dielectric measurements for gold.⁴⁷ For each simulation, the incident source had a given polarization state (linear, radial, or azimuthal) and a Gaussian temporal envelope chosen to span the incident wavelengths from 500 to 1000 nm. A spatial envelope was chosen to give each beam a 300 nm diameter (for the linearly polarized beam, this is the width of the Gaussian; for the CVBs, this is the mean diameter of the doughnut). A perfectly matched layer was used at the boundary of the simulation domain to model an open system. The simulation was then time-stepped until the fields decayed and the scattering spectra converged. Figure 4a shows a diagram of the simulation box.

The scattered electric field components were collected on the surface of a spherical monitor that encompassed the Au nanoparticle dimer. These electric field components were used to compute a multipole expansion of the scattered radiation by projecting the electric field onto a set of orthogonal vector spherical harmonic wave (VSHW) functions^{48–50}

$$a_{nm} = \frac{\int_0^{2\pi} \int_0^\pi \mathbf{E}_{\text{scat}} \cdot \mathbf{N}_{nm}^* \sin \theta \, d\theta \, d\phi}{\int_0^{2\pi} \int_0^\pi |\mathbf{N}_{nm}|^2 \sin \theta \, d\theta \, d\phi} \quad (1)$$

$$b_{nm} = \frac{\int_0^{2\pi} \int_0^\pi \mathbf{E}_{\text{scat}} \cdot \mathbf{M}_{nm}^* \sin \theta \, d\theta \, d\phi}{\int_0^{2\pi} \int_0^\pi |\mathbf{M}_{nm}|^2 \sin \theta \, d\theta \, d\phi} \quad (2)$$

Here, a_{nm} and b_{nm} are the electric and magnetic multipole scattering coefficients, respectively, of order n and spherical orientation m . Physically, $n = 1$ corresponds to the dipole modes, $n = 2$ corresponds to the quadrupole modes, etc., and $m = -n, -n + 1, \dots, 0, \dots, n - 1, n$ specifies different orientations of the mode. The complex vector fields \mathbf{N}_{nm} and \mathbf{M}_{nm} are the electric and magnetic VSHW functions, respectively.

The total scattering cross-section is then computed as a sum over the individual multipolar scattering coefficients

$$C_{\text{sca}} = k^2 \sum_{n=1}^{\infty} \sum_{m=-n}^n n(n+1) (|a_{nm}|^2 + |b_{nm}|^2) \quad (3)$$

Here, k is the wavenumber of the incident radiation in the oil medium. Each term in the sum represents the multipolar scattering cross-section of a particular multipolar mode.

This method was used for radiation up to quadrupole order for both electric and magnetic modes. Figure 3 shows the multipole expansion results for the AuNP dimer with a 40 nm gap. Equations 1 and 2 also allow the fields to be projected into the far field, from which angular scattering quantities can be computed. To determine spectra in the back-scattering direction

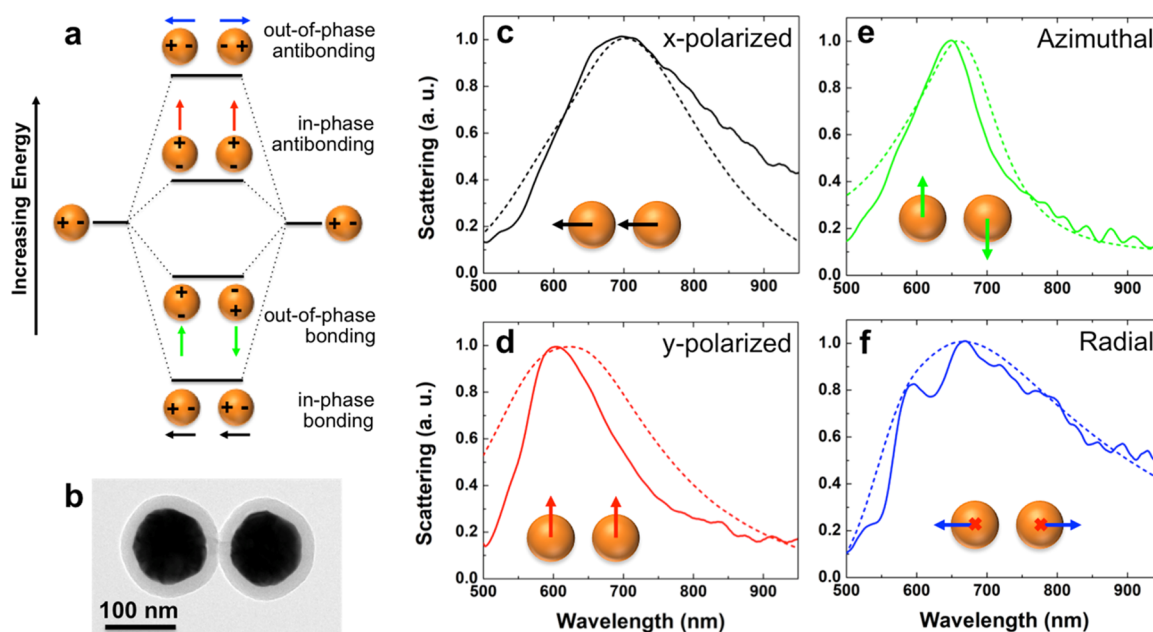


Figure 2. Plasmon hybridization model along with measured and simulated scattering spectra of a AuNP dimer excited by linear, azimuthal, and radial polarized beams. (a) Scheme of the plasmon hybridization model of a symmetric dimer, depicting in-phase/out-of-phase bonding/antibonding combinations of dipole moments. The arrows in the scheme indicate the dipole moments of the individual particles. The colors are matched to the types scalar or vector beams used, as shown in (c–f). (b) A TEM image of a AuNP dimer of 100 nm diameter coated and separated by silica shells, with 20 nm shell thickness (40 nm gap). (c–f) Experimental (solid) and simulated (dashed) scattering spectra of the AuNP dimer illuminated by tightly focused linear beams parallel ((c) *x*-polarized) and perpendicular ((d) *y*-polarized) to the dimer axis and azimuthal (e) and radial (f) beams, respectively. The arrows in (c–f) indicate the instantaneous direction of the electric field acting on the AuNP center at the focal plane (*xy* plane) and the dipoles thereby induced. The two red crosses in (f) indicate the electric field is in the *z*-direction (*xz* plane), which is the beam propagation direction.

to mimic the experiments, the far-field Poynting vector is integrated over the cap of a cone with apex angle 140° , oriented in the backward direction. Figure 2 shows simulated back-scattering spectra in comparison with experiment.

To use smaller mesh sizes, FDTD simulations of nearly touching AuNP dimers were carried out with commercial software (FDTD Solutions 8.18, Lumerical Inc.). A total-field scattered-field source was used to simulate a propagating plane wave interacting with the AuNP dimers, with a wavelength range of 500–1200 nm. Both longitudinal and transverse LSPR were calculated by setting the illumination polarization parallel or perpendicular to the dimer axis. A three-dimensional nonuniform mesh was used, and grid sizes of 0.2 nm (in *x*- and *y*-axis) and 0.5 nm (in *z*-axis) were chosen for the AuNP dimers. The size of AuNP is 100 nm in diameter. We simulated AuNPs dimers with gaps of 1.0, 0.8, 0.6, and 0.4 nm. The results are shown in Figures S5b and S2.

Scattering spectra of individual AuNP@SiO₂ and AuNP were calculated using Mie theory.⁵¹ The sizes of AuNPs were obtained from TEM images. The effective refractive index (*n*) of environment used for Au@SiO₂ is 1.47 (between SiO₂ (*n* = 1.45) and immersion oil (*n* = 1.51)) and for AuNP is 1.51 (index of immersion oil). The results are shown in Figure S3.

RESULTS AND DISCUSSION

Setup for Single-Particle Spectroscopy and Beam Profiles. All single-particle optical studies were performed with a home-built microscopy setup shown in Figure 1a. We used a supercontinuum fiber laser source (500–1200 nm, Fianium) to illuminate the nanoparticle samples. Either the conventional zero-order Gaussian mode (LP) or higher-order

Hermite–Gaussian doughnut modes (AP and RP) were used. The broadband AP and RP beams were created using a vector beam generator (ARCOptix), a liquid-crystal-based polarization converter that uses twisted nematic liquid crystals sandwiched between one uniform and one circularly rubbed alignment layer.⁴⁴ The vector beam generator was positioned on a translation stage outside of the microscope. The collimated beam was reflected by a 50:50 beam splitter and focused by an oil immersion objective onto the nanoparticles supported on a TEM grid inside a liquid-filled sample cell. The back-scattered images and spectra of the sample plane were recorded (in reflection) by a CMOS camera and a spectrometer CCD array detector (Andor). A halogen light source was used for imaging the samples in bright field microscopy. Figure 1b–d shows optical microscope images (left column; measured in the forward direction) and simulated beam profiles (right column) of the LP, AP, and RP beams.^{33,50} Figure 1e shows the intensity profiles of the red rectangular area of the AP beams noted in Figure 1c.

Samples were prepared by drop-casting the silica-coated AuNP (AuNP@SiO₂, nanoComposix) or AuNP aqueous suspension on a TEM finder grid and dried overnight. TEM images of AuNP dimers were taken before the measurement. The grid was embedded in immersion oil and sandwiched by two glass cover slides. Thus, the refractive index of the space between the coverslip and grid is nearly matched to them, and the scattering from the oil/formvar interface is very weak. More experimental details can be found in Methods.

Plasmon Hybridization Model of the AuNP Dimer. The plasmon modes expected from the hybridization model^{17–19,52} for a symmetric AuNP dimer oriented along the *x*-axis are shown

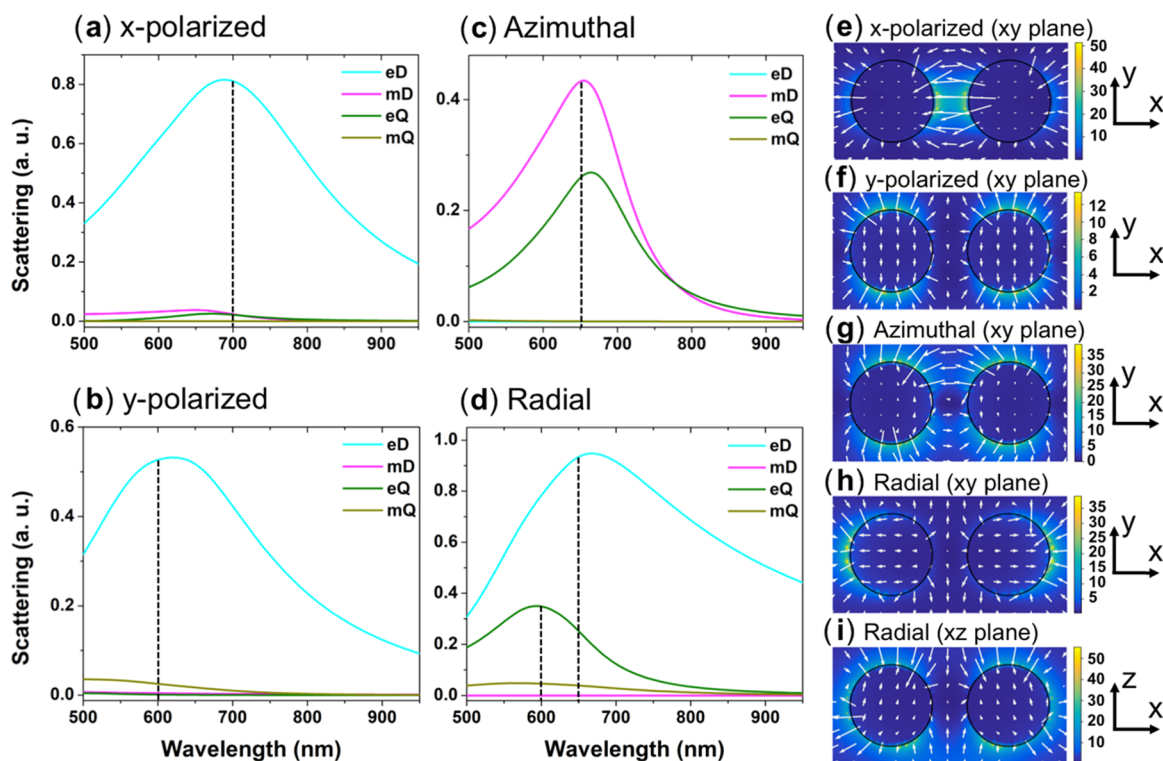


Figure 3. Expansion of the FDTD scattering amplitudes into electric and magnetic multipolar modes and near-field intensity distributions for (a, e) *x*-polarized, (b, f) *y*-polarized, (c, g) azimuthally polarized, and (d, h, and i) radially polarized beam excitation. The resonance peaks are at (a) 699 nm (eD), (b) 621 nm (eD), (c) 655 nm (mD) and 664 nm (eQ), and (d) 594 nm (eQ), and 668 nm (eD). Although the LP beams only excite eD modes, the CVBs can excite eQ and/or mD modes. For radial beam illumination, the resonances of eD and eQ modes are well separated; a splitting of the peak was observed in the experimental spectra (Figure 2f solid). The dashed lines in (a–d) indicate the wavelengths selected for the near-field intensity distributions shown in (e–i). (e–h) The field distribution in the *xy* plane (focal plane) and (i) the field distribution in the *xz* plane associated with the electric dipole (eD) mode in the *z*-direction for radial beam excitation. The white arrows in (e–i) indicate the local electric field polarization, and the $|E|^2$ intensities are quantified with the color scales.

in Figure 2a. When the incident beam is polarized along the dimer axis, the in-phase coupling forms a bonding state with a red-shifted resonance (Figure 2a, parallel-directed black arrows), and the out-of-phase coupling represents an antibonding state with a blue-shifted resonance (Figure 2a, oppositely directed blue arrows). The scenario is just the opposite for polarization perpendicular to the dimer axis. The in-phase coupling is an “antibonding” state with a blue-shifted resonance (Figure 2a, parallel-directed red arrows), whereas the out-of-phase coupling with red-shifted resonance is a “bonding” state (Figure 2a, oppositely directed green arrows). After coupling, the bonding mode is lower energy, and the antibonding mode is higher energy. In addition, the coupling is weaker for polarization perpendicular to the dimer axis.¹⁸ Therefore, plasmon coupling of a symmetric AuNP dimer can form four states: in-phase bonding, out-of-phase bonding, in-phase antibonding, and out-of-phase antibonding, ordered from lower to higher energy. LP illumination of a symmetric AuNP dimer only allows excitation of in-phase bonding (*x*-polarized) or antibonding state (*y*-polarized) states due to the cancellation of the oppositely oriented dipole moments (in near-field proximity and neglecting retardation).

Spectra of a AuNP Dimer with 40 nm Gap. We measured a AuNP dimer consisting of 100 nm diameter AuNPs oriented along the *x*-axis with a gap of 40 nm (Figure 2b). This particular gap can be realized by using silica-coated AuNPs with a silica shell thickness of 20 nm. For the same dimer, we measured four spectra using *x*-polarized, *y*-polarized, AP, and RP beams. The

results are shown in Figure 2c–f. We also measured the scattering spectra of several individual AuNP@SiO₂ nanoparticles for comparison. Measured single AuNP scattering spectra and the spectra obtained from Mie theory are shown in Figure S3a. They exhibit LSPRs at 610 nm. The plasmon resonance of the AuNP dimer is red shifted to 699 nm for *x*-polarized beam illumination (Figure 2c, parallel to the dimer axis). This corresponds to the in-phase bonding state, the lowest energy state in plasmon hybridization. When the beam is *y*-polarized (Figure 2d, perpendicular to the dimer axis), the resonance undergoes a small blue shift to 603 nm corresponding to an in-phase antibonding state. In the case of AP beam excitation, the spectrum exhibits a resonance at 649 nm (Figure 2e). In this case, the field distribution at the focal plane indicates that the field acting on the particles is primarily perpendicular to the dimer axis, but with opposite directions in each particle. Therefore, we associate this plasmon resonance with the out-of-phase bonding state with the two dipole moments perpendicular to the dimer axis (and mutually antiparallel). The plasmon resonance is narrower than the bright modes, consistent with this being a dark mode. Finally, when the AuNP dimer is illuminated by the RP beam, the spectrum shows two main resonances at 586 and 669 nm (Figure 2f). At the focal plane of the focused RP beam, the field acting on each particle is now parallel to the dimer axis, but with opposite directions (antiparallel) in each particle. Therefore, the resonance at 586 nm is assigned to be the out-of-phase antibonding state, i.e., the highest energy in the model. Interestingly, the RP beam also has

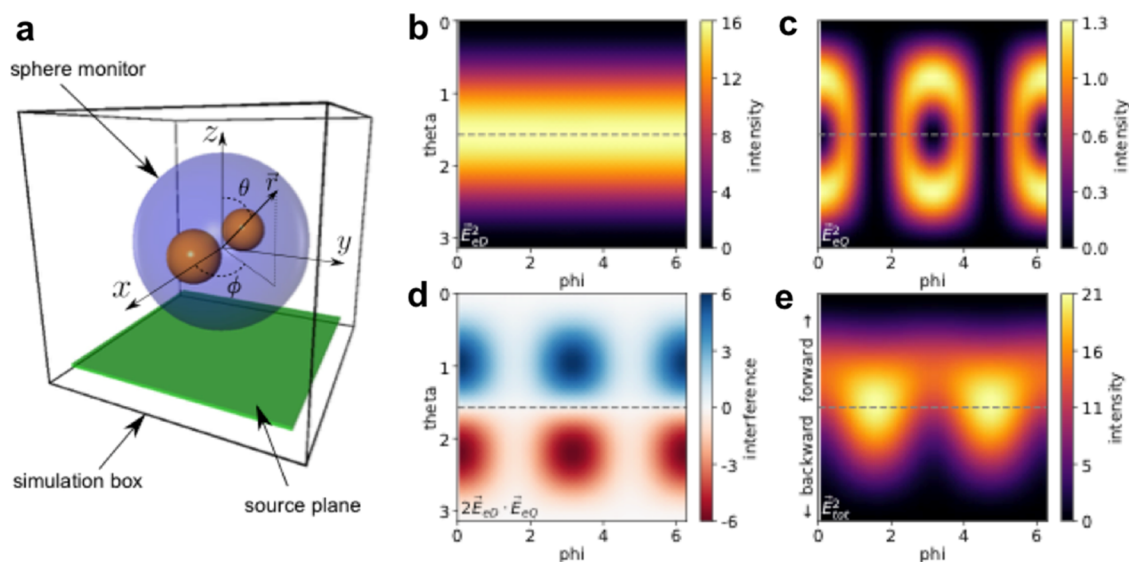


Figure 4. Simulation setup and angular scattering distributions measured in simulations of the AuNP dimer under radial beam illumination. (a) Scheme of the FDTD simulation box. A source is propagated from the green plane in the $+z$ -direction. The AuNP dimer is placed at the center of the simulation box and the dimer axis is along the x -axis. The blue sphere surrounding the AuNP dimer is a special spherical monitor that collects the scattered electric field, including magnitude, polarization, and phase information. The data collected from this monitor are used in the multipole expansion described in [Methods](#). The angles θ (θ) and ϕ (ϕ) are shown in the scheme. (b) Angular scattering of a z -oriented eD mode. (c) Angular scattering of the eQ mode. (d) Angular scattering of the interference term between eD and eQ modes. Red denotes destructive interference and blue denotes constructive interference. (e) Total angular scattering of the AuNP dimer. The interference between the eD and eQ modes creates a spatial interference pattern that partially destructively interferes in the backward direction, which is the direction of the experimental measurements.

a longitudinal z -directed electric field component at the focus centered and oriented along the optical axis.⁵³ This longitudinal electric field can induce an in-phase coupling of electric dipole moments in the z -direction (indicated as two red crosses in [Figure 2f](#)), yet gives rise to the red-shifted resonance at 669 nm. Since this longitudinally polarized case is complex due to beam propagation, we model and discuss this dual resonance phenomenon under radial beam illumination in the next subsection.

Electrodynamics Simulations: Scattering Spectra, Multipole Expansion, and Near-Field Intensity Distributions. To get a deeper insight into the dark plasmon modes excited by CVBs, we performed electrodynamics simulations on AuNP dimers.^{33,50} The simulation results of scattering spectra shown in [Figure 2](#) (dashed curves) were performed with the same Au core diameters and SiO₂ shell thickness as were determined from the corresponding TEM image ([Figure 2b](#)), using a 2 nm grid cell resolution. Simulations were performed with the FDTD method, using the MEEP software package.⁴⁶ The simulated spectra presented are for a back-scattering geometry with a specific angular range that closely corresponds to our experimental setup and numerical aperture of the objective.⁵⁰ [Figure 2c–f](#) shows that the experimental (solid) and simulated (dashed) scattering spectra of the AuNP dimer are in very good agreement with well-matched resonance maxima and widths for each polarized light illumination condition.

Understanding the spectral features excited by different types of polarized light requires that we assign an identity to them. To do this, we perform a near-to-far-field transformation of the scattered fields and project the far fields into their electric and magnetic multipolar (dipolar and quadrupolar) contributions (more details of the multipole expansion is provided in [Methods](#)). We obtain the multipolar electric and/or magnetic modes that give rise to the total scattering ([Figure 3](#)) for the four different beams. Each simulated spectrum in [Figure 2](#) is

decomposed into the four lowest order multipolar modes: electric dipole (eD), magnetic dipole (mD), electric quadrupole (eQ), and magnetic quadrupole (mQ), as shown in [Figure 3a–d](#). Our FDTD simulations of the AuNP dimer allow the following assignments: (i) only the eD mode is excited by LP light. For x -polarized light, the resonance of the eD mode is at 699 nm ([Figure 3a](#)) and for y -polarized light, the resonance of the eD mode is at 621 nm ([Figure 3b](#)); (ii) AP beams exclusively excite (and scatter from) mD (655 nm) and eQ (664 nm) modes ([Figure 3c](#)). Interestingly, these two modes have almost the same resonance (only ~ 10 nm difference) and line width, and therefore cannot be distinguished experimentally; (iii) RP beams excite eQ (594 nm) and eD (668 nm) modes ([Figure 3d](#)). The larger spectral difference (~ 80 nm) in these resonances explains their splitting in the scattering spectra obtained by radial beam excitation ([Figure 2f](#)).

In addition to expansion of the scattering attitudes into multipolar modes, it is also possible to obtain the near-field $|E^2|$ intensity distributions (with electric field polarization) and surface charge distributions excited in the AuNP dimer from electrodynamics simulations. The near-field intensity distributions are shown in [Figures 3e–h](#) with arrows indicating the electric field polarization for each polarized light illumination condition at wavelengths near the plasmon resonances. For x -polarized light ([Figure 3e](#)), the arrows indicate that the plasmon coupling is in-phase along the x -axis, and a hot spot is formed in the gap region due to the large accumulation of opposite electric charges facing the dimer gap.⁵⁴ y -polarized light ([Figure 3f](#)) also produces an in-phase electric dipolar coupling, but along the y -axis, and the near-field distribution is mainly at the top and bottom regions of each AuNP. The collective excitation is very similar to the field distribution of two individual electric dipoles oriented along the y -axis (in the quasistatic approximation), indicating weak plasmon coupling for y -polarized illumination.

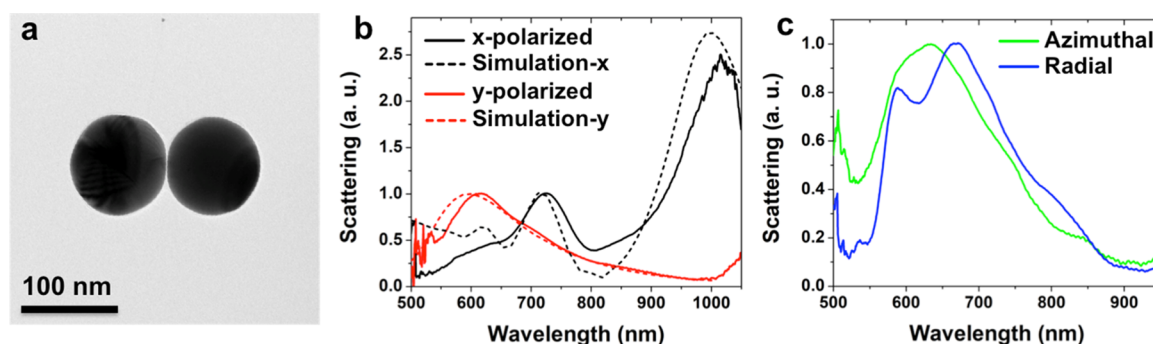


Figure 5. Measurements and FDTD simulations of the scattering spectra of an almost touching AuNP dimer excited by scalar (linear) beams and vector beams. (a) A TEM image of a 100 nm AuNP dimer with sub-nanometer gap. (b) Experimental (solid) and simulated (dashed) scattering spectra of the AuNP dimer in (a), excited by linear beams parallel (*x*-polarized, black) and perpendicular (*y*-polarized, red) to the dimer axis. The gap of the AuNP dimer is 0.6 nm in the simulations. (c) Experimental scattering spectra of the AuNP dimer excited by azimuthally (green) and radially (blue) polarized beams.

For azimuthal beam excitation (Figure 3g), the electric field acts along the *y*-axis of the AuNPs, but the field polarizations on each AuNP are opposite (antiparallel), resulting in an out-of-phase coupling and inducing an eQ mode. Furthermore, the electric field polarization between the two particles is basically along the *y*-axis, forming an instantaneous curl of displacement current in the *xy* plane. Therefore, a mD mode oriented along the *z*-axis is excited. Since both the eQ and mD modes share similar electric field distributions, their spectra (plasmon resonances) are nearly overlapped (Figure 3c).

Finally, due to the longitudinal electric field component (*z*-direction), the radial beam excitation drives multiple modes along the *z*-axis and in the *xy* plane. Both transverse (*xy* plane, Figure 3h) and longitudinal (*xz* plane, Figure 3i) near-field intensity distributions are shown. First, the electric field in the *xy* plane is along the *x*-axis of the AuNPs with opposite (antiparallel) polarizations, forming an eQ by out-of-phase coupling. However, the field distribution is mainly on two distal sides of the AuNP dimer. Second, the excitation along the *xz* plane is an in-phase coupling of two electric dipoles oriented along the *z*-axis. Superficially, this is similar to the case of *y*-polarized light, which involves in-phase coupling of electric dipole moments. However, the field distributions excited by the radial beam are quite different compared to the excitation by the *y*-polarized (LP) beam. The electric field polarization on each AuNP for RP beam is not perfectly parallel to each other, and the field distribution is more extended about the AuNP surface (Figure 3i), resulting in a spectrally broader eD mode and red-shifted resonance (Figure 3d). We summarize the near-field intensity distributions and local electric field polarization for each polarization of light at near-resonance wavelengths in Figure S4 in the Supporting Information.

Angular Scattering Distributions under CVBs Illumination. We calculated the far-field angular scattering patterns of the AuNP dimer for different CVB illumination conditions. A spherical monitor that collects the scattered fields is placed at the center of the simulation box and encloses the dimer pair (Figure 4a). The angular scattering intensity is then calculated as a function of the angles theta (θ) and phi (ϕ). The angular scattering can also be decomposed into its individual multipolar component contributions. Figure 4b–e shows the angular scattering patterns for RP beam illumination, and the angular scattering for AP beam illumination is shown in Figure S5. For the RP beam, the electric dipole is *z*-oriented (Figure 4b). The angular scattering of the electric quadrupolar mode has a more

complex pattern than the dipole mode and a maximum intensity an order of magnitude weaker (Figure 4c).

Despite the weaker eQ mode, there is a non-negligible interference term between the eD and eQ modes. This interference pattern causes destructive interference in the back-scattering direction and constructive interference in the forward scattering direction (Figure 4d). The total angular scattering intensity is then the sum of the individual multipolar intensities and their interference (Figure 4e). The result is an angular scattering pattern that is skewed in the forward scattering direction. For AP beam illumination, a similar interference effect occurs between the mD and eQ modes. In this case, however, the destructive interference occurs at the azimuthal angles $\phi = \pi, 3\pi/2$, which corresponds to the *y*-axis (perpendicular to the dimer axis), whereas the back-scattering and forward scattering are the same.

Scattering Spectra of Nearly Touching AuNP Dimers.

Given the significant spectral shifts and coupling for AuNP dimers with 40 nm separation, we studied the effect of the gap distance on the scattering spectra of AuNP dimers. We used “bare” AuNPs with diameter of 100 nm so the two AuNPs in the dimer are nearly touching (<1 nm separation). It is expected that the coupling should be stronger than that of the dimer with 40 nm gap. Figure 5 shows the scattering spectra of a nearly touching AuNP dimer oriented along the *x*-axis with *x*-polarized, *y*-polarized, AP, and RP light excitations. For comparison, scattering spectra of individual AuNPs were also measured. The experimental results and Mie-calculated spectra of an individual AuNP shown in Figure S3b have a LSPR at 628 nm. For *x*-polarized beam excitation (Figure 5b, black solid curve), in addition to a broad shoulder in the 600 nm region and a resonance at 723 nm, there is a new pronounced resonance at 1015 nm. The new resonance in the nearly touching AuNP dimer has also been reported in lithographically patterned AuNP dimers⁵⁵ and theoretically for nearly touching AuNP dimers calculated using the boundary element method.⁵⁴ When the gap distance, *d*, is decreased to the nearly touching regime ($d/a < 0.005$, *a* is the diameter of AuNP), the plasmon modes were shown to strongly shift toward the infrared.⁵⁴

For *y*-polarized excitation (Figure 5b, red solid curve), the response is an in-phase antibonding state with a resonance at 617 nm, which is close to the LSPR of individual AuNP because of the weak plasmon coupling in the transverse (*y*-) direction. For the cases of AP and RP beam excitation, the spectra are very similar to the case of AuNP dimers with 40 nm gap, but with

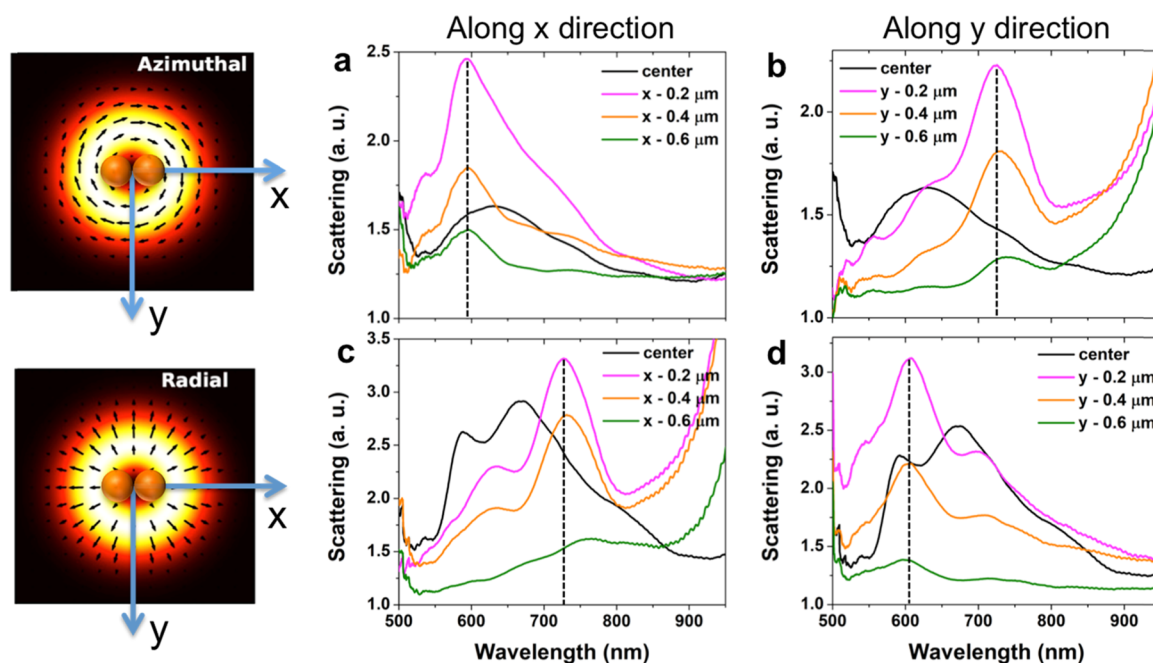


Figure 6. AuNP dimer (sub-nanometer gap) spectra at different x - and y -positions with respect to the beam axis. (a, b) Scattering spectra for azimuthal beam illumination while moving the AuNP dimer in the x - (a) and y - (b) directions. (c, d) Scattering spectra for radial beam illumination while moving the Au dimer in the x - (c) and y - (d) directions. The left panels schematically indicate the directions of the spatial shifts along the x - and y -directions. The spectra in (a)–(d) shown as solid black curves are obtained at the center positions. The dashed black lines indicate the peak positions for dimers spatially shifted off the center. The particle and beam sizes shown in the left panels are from the actual simulation indicating their spatial overlay.

slight resonance shifts. When the AuNP dimer is excited by AP beams, the resonance is at 634 nm. By contrast, the spectra show two resonances at 589 and 668 nm for RP beam excitation. As discussed before, the spectra obtained from AP beam excitation are eQ and mD modes, which are nearly overlapped, whereas the spectra obtained from RP beam excitation are an eQ mode in the transverse plane (589 nm) and a longitudinal eD mode along the z -axis (668 nm).

To perform electrodynamics simulations on the nearly touching AuNP dimer, the FDTD grid cell needs to be in sub-nanometer. Therefore, the simulations were performed with Lumerical (FDTD Solutions), since finer grids as small as 0.2 nm can be used, and adaptive mesh sizes are possible. We simulated x -oriented AuNP dimers using 0.2 nm grid cells, with gaps of 1.0, 0.8, 0.6, and 0.4 nm. The illumination is either x -polarized or y -polarized light. The results for a 0.6 nm gap are shown in Figure 5b (dashed curves), and full results are in Figure S2. Three resonances at 615, 710, and 1000 nm are found for the spectrum under x -polarized (linearly polarized) excitation. By contrast, y -polarized illumination only gives a resonance at 600 nm. The experimental results are consistent with the simulated results for a 0.6 nm gap, with slight resonance shifts (~ 15 nm). Therefore, we conclude that the gap of this nearly touching AuNP dimer is about 0.5–0.6 nm. Since choices of the polarization of light are limited in Lumerical Solutions, we did not perform simulations with CVBs' illumination.

Position-Dependent Scattering Spectra when Shifting the Dimer from the CVB Axis. To further investigate the illumination by CVBs, we broke the cylindrical symmetry of the illumination by shifting the AuNP dimer off the center of the CVBs. One can envision that the illumination becomes like a linearly polarized beam since the sample interacts preferentially or exclusively with an arc of the CVBs. We measured the scattering spectra of the same AuNP dimer (Figure 5a) using LP,

AP, and RP light, but with small shifts of the AuNP dimer along the x - or y -directions with respect to the beam axis. We chose this nearly touching AuNP dimer as an example since the resonance shifts are more pronounced due to stronger coupling for the small gap. The intensity decreased while moving off the center for LP light illumination (both x -polarized and y -polarized), without any resonance shift (Figure S6). These findings can be attributed to the spatially homogeneous polarization and Gaussian intensity distribution for LP beams. Interestingly, the main resonance shifted to about 600 nm (Figure 6a) for AP beam excitation as the AuNP dimer was moved along the x -axis, eventually becoming very similar to the spectrum obtained with y -polarized light excitation (Figure 5b, red solid curve). When the AuNP dimer was moved along the y -axis, the resonance shifted to about 725 nm (Figure 6b), which is similar to the x -polarized light excitation (Figure 5b black solid curve). The diverse shifts of the resonances are ascribed to the inhomogeneous spatial polarization. When shifted along the x -axis, the AuNP dimer only “felt” an arc of the AP beam, with polarization perpendicular to the dimer axis. Conversely, when shifted along the y -axis, the AuNP dimer was in a region of the polarization parallel to the dimer axis. In addition to the resonance shifts, the signal intensity initially increased when shifting the AuNP dimer away from the center due to the annular intensity profile of the AP beam (Figure 1c). For RP beam excitation, the features were similar to the case of AP beam excitation, but the shifts of the resonances were in the opposite directions. This is the expected behavior since the spatial polarization of azimuthal and radial beams are everywhere perpendicular to each other.

Gap-Dependent Scattering Spectra of AuNP Dimers. To further investigate the properties of AuNP dimers illuminated by CVBs, we have investigated scattering spectra of the AuNP dimers with different gap distances. To change the

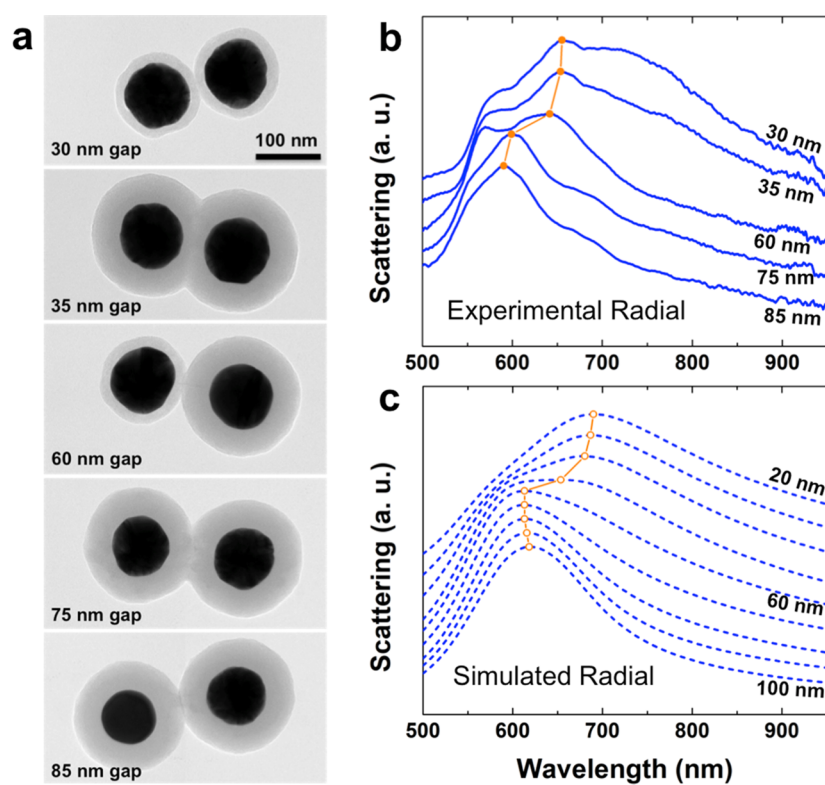


Figure 7. Scattering spectra of AuNP dimers with different gap distances. (a) TEM images of AuNP dimers, from top to bottom, with gaps of 30, 35, 60, 75, 85 nm. (b) Experimental scattering spectra of AuNP dimers (shown in (a)) with radial polarized (RP) beam excitation. (c) Simulated scattering spectra of AuNP dimers by RP beam excitation, with gaps from 20 to 100 nm (10 nm step size). The orange symbols and lines in (b) and (c) indicate the main resonances of the spectra.

gap distances between the AuNPs, we etched the silica shell (decreased the gap) or grew a new layer on the original silica surface (increased the gap). More experimental details can be found in [Methods](#). In this way, we obtained AuNP dimers with gaps from 30 to 85 nm. [Figure 7a](#) shows several AuNP dimers with gaps of 30, 35, 60, 75, and 85 nm. We measured the scattering spectra using LP (both x - and y -polarized), AP, and RP light for each dimer. Their corresponding scattering spectra are shown in [Figures 7b](#) and [S7](#). While increasing the gap distances, the resonances do not shift for y -polarized and azimuthally polarized light ([Figure S7b,c](#)) since the electric dipole on each AuNP is perpendicular to the dimer axis, and thus not sensitive to the change of the gap distance. By contrast, the resonances blue shifted while increasing the gap distances for x -polarized light and radially polarized light. The blue-shift of the resonances can be attributed to the weaker plasmonic coupling at larger gap distances. In the case of radially polarized light, in addition to the blue shift of the main resonances, the spectra become more symmetric at larger gap distances.

We performed electrodynamic simulations on AuNP dimers to understand these experimental findings for changing gap distances. The simulated AuNP dia. is 100 nm, and the gap distances are varied from 20 to 100 nm with a step size of 10 nm. The simulated spectra are shown in [Figures 7c](#) and [S7](#). The trends of the scattering spectra are very consistent with the experimental spectra. The small mismatch of the resonances can be attributed to the nonspherical shapes and variable AuNP sizes in the experiments. The multipole expansion analysis at 100 nm gap distance is shown in [Figure S8](#). Compared to the case of 40 nm gap distances, each electric/magnetic mode is similar for LP and AP excitations. However, we found that the electric dipole

mode for RP illumination to be blue-shifted and well overlapped with the electric quadrupole mode. This result explains why the RP measured spectra become more symmetric at larger gap distances.

CONCLUSIONS

We demonstrated that CVB illumination of symmetric AuNP dimers enables excitation of dark plasmon modes. These results for symmetric dimers are, we believe, the first direct experimental validation of the plasmon hybridization model.^{17–19,52} The hybridized states are also interpreted in terms of electric and magnetic multipolar modes. In cases with out-of-phase plasmonic coupling, we found that magnetic dipolar and electric quadrupolar modes are induced. These multipolar modes are found to spatially interfere with each other in the far field thereby affecting the directional scattering spectra. Furthermore, shifting the AuNP dimer off the center of the CVBs causes the spectra to change to become like those measured by linear beam excitation, as intuitively expected.

We also uncovered novel excitations in the longitudinal direction (i.e., beam propagation). The focused azimuthal CVB has a pure optical magnetic field on-axis that exclusively excites magnetic modes (zero electric field at the center of inversion). By contrast, the focused radial CVB has a longitudinally polarized electric field that excites a pure electric dipole mode (zero magnetic field at the center of inversion) at the focus. The latter is spectrally sharp and spatially centered along the optical axis.^{53,56} Simulations (not shown) indicate that the unique properties of focused azimuthal and radial beams could excite pronounced dark plasmon modes in longitudinal-oriented AuNP dimers, where only magnetic or electric modes hybridize.

However, this is a geometry we did not investigate experimentally.

Given the novel excitations we found for AuNP dimers, it would be interesting to investigate other nanostructures with longitudinal geometries with CVBs' illumination. Our work also opens new opportunities for spectroscopic investigation of dark modes and Fano resonances in other symmetric plasmonic nanostructures composed of anisotropic nanoparticles, e.g., Au nanorods. The anisotropic shapes would give rise to larger plasmon resonance shifts and new plasmon-coupled resonances with higher-order multipolar modes.

■ ASSOCIATED CONTENT

Supporting Information

The Supporting Information is available free of charge on the ACS Publications website at DOI: 10.1021/acs.jpcc.8b10415.

Scattering spectra of individual Au@SiO₂ nanoparticle and AuNP; near-field distribution of all polarizations at different wavelengths; angular scattering distributions of sub-nanometer AuNP dimer illuminated by azimuthal beam; FDTD simulations of nearly touching AuNP dimer by linearly polarized light; spectra of positioning shift illuminated by x -polarized and y -polarized light; spectra of gaps from 30 to 85 nm; multipole expansion analysis of 100 nm gap AuNP dimer (PDF)

AuNP dimer shifted from left side to the right side of the vector beams (AVI)

■ AUTHOR INFORMATION

Corresponding Author

*E-mail: nfschere@uchicago.edu.

ORCID

Tian-Song Deng: 0000-0002-0841-4932

Yuval Yifat: 0000-0003-0952-556X

Author Contributions

[†]T.-S.D. and J.P. contributed equally to this work.

Author Contributions

T.-S.D. and J.P. contributed equally to this work. T.-S.D. and N.F.S. designed the research; T.-S.D. performed the experimental measurements; J.P. and Y.Y. performed the simulations; N.S. helped in performing measurements; T.-S.D., J.P., N.S., and Y.Y. analyzed the data; T.-S.D., J.P., and N.F.S. wrote the manuscript; N.F.S. supervised the project; and all authors discussed the results and commented on the manuscript.

Notes

The authors declare no competing financial interest.

■ ACKNOWLEDGMENTS

We thank Dr Stephen K. Gray for helpful conversations on electrostatics simulations and analysis. The authors acknowledge support from the Vannevar Bush Faculty Fellowship program sponsored by the Basic Research Office of the Assistant Secretary of Defense for Research and Engineering and funded by the Office of Naval Research through grant N00014-16-1-2502. We also acknowledge the University of Chicago NSF MRSEC for central facilities use. We thank the University of Chicago Research Computing Center for a grant of computer time for the FDTD simulations reported here. The simulations using Lumerical were performed at the Center for Nanoscale Materials, a U.S. Department of Energy Office of Science User

Facility and supported by the U.S. Department of Energy, Office of Science, under Contract No. DE-AC02-06CH11357.

■ REFERENCES

- (1) Novotny, L.; Hecht, B. *Principles of Nano-Optics*; Cambridge University Press, 2006.
- (2) Maier, S. A. *Plasmonics: Fundamentals and Applications*; Springer, 2007.
- (3) Halas, N. J.; Lal, S.; Chang, W.-S.; Link, S.; Nordlander, P. Plasmons in strongly coupled metallic nanostructures. *Chem. Rev.* **2011**, *111*, 3913–3961.
- (4) Sönnichsen, C.; Reinhard, B. M.; Liphardt, J.; Alivisatos, A. P. A molecular ruler based on plasmon coupling of single gold and silver nanoparticles. *Nat. Biotechnol.* **2005**, *23*, 741–745.
- (5) Jain, P. K.; Huang, W. Y.; El-Sayed, M. A. On the universal scaling behavior of the distance decay of plasmon coupling in metal nanoparticle pairs: A plasmon ruler equation. *Nano Lett.* **2007**, *7*, 2080–2088.
- (6) Liu, N.; Hentschel, M.; Weiss, T.; Alivisatos, A. P.; Giessen, H. Three-Dimensional Plasmon Rulers. *Science* **2011**, *332*, 1407–1410.
- (7) Willets, K. A.; Van Duyne, R. P. Localized surface plasmon resonance spectroscopy and sensing. *Annu. Rev. Phys. Chem.* **2007**, *58*, 267–297.
- (8) Lim, D. K.; Jeon, K. S.; Kim, H. M.; Nam, J. M.; Suh, Y. D. Nanogap-engineerable Raman-active nanodumbbells for single-molecule detection. *Nat. Mater.* **2010**, *9*, 60–67.
- (9) Arroyo, J. O.; Kukura, P. Non-fluorescent schemes for single-molecule detection, imaging and spectroscopy. *Nat. Photonics* **2016**, *10*, 11–17.
- (10) Lee, H.; Lee, J. H.; Jin, S. M.; Suh, Y. D.; Nam, J. M. Single-Molecule and Single-Particle-Based Correlation Studies between Localized Surface Plasmons of Dimeric Nanostructures with similar to 1 nm Gap and Surface-Enhanced Raman Scattering. *Nano Lett.* **2013**, *13*, 6113–6121.
- (11) Kinkhabwala, A.; Yu, Z. F.; Fan, S. H.; Avlasevich, Y.; Mullen, K.; Moerner, W. E. Large single-molecule fluorescence enhancements produced by a bowtie nanoantenna. *Nat. Photonics* **2009**, *3*, 654–657.
- (12) Schietinger, S.; Aichele, T.; Wang, H. Q.; Nann, T.; Benson, O. Plasmon-Enhanced Upconversion in Single NaYF₄:Yb³⁺/Er³⁺ Codoped Nanocrystals. *Nano Lett.* **2010**, *10*, 134–138.
- (13) Large, N.; Abb, M.; Aizpurua, J.; Muskens, O. L. Photoconductively Loaded Plasmonic Nanoantenna as Building Block for Ultracompact Optical Switches. *Nano Lett.* **2010**, *10*, 1741–1746.
- (14) Kuzyk, A.; Schreiber, R.; Fan, Z. Y.; Pardatscher, G.; Roller, E. M.; Hoge, A.; Simmel, F. C.; Govorov, A. O.; Liedl, T. DNA-based self-assembly of chiral plasmonic nanostructures with tailored optical response. *Nature* **2012**, *483*, 311–314.
- (15) Grigorenko, A. N.; Roberts, N. W.; Dickinson, M. R.; Zhang, Y. Nanometric optical tweezers based on nanostructured substrates. *Nat. Photonics* **2008**, *2*, 365–370.
- (16) Kawata, S.; Ono, A.; Verma, P. Subwavelength colour imaging with a metallic nanolens. *Nat. Photonics* **2008**, *2*, 438–442.
- (17) Prodan, E.; Radloff, C.; Halas, N. J.; Nordlander, P. A hybridization model for the plasmon response of complex nanostructures. *Science* **2003**, *302*, 419–422.
- (18) Nordlander, P.; Oubre, C.; Prodan, E.; Li, K.; Stockman, M. I. Plasmon hybridization in nanoparticle dimers. *Nano Lett.* **2004**, *4*, 899–903.
- (19) Sheikholeslami, S.; Jun, Y. W.; Jain, P. K.; Alivisatos, A. P. Coupling of Optical Resonances in a Compositionally Asymmetric Plasmonic Nanoparticle Dimer. *Nano Lett.* **2010**, *10*, 2655–2660.
- (20) Brown, L. V.; Sobhani, H.; Lassiter, J. B.; Nordlander, P.; Halas, N. J. Heterodimers: Plasmonic Properties of Mismatched Nanoparticle Pairs. *ACS Nano* **2010**, *4*, 819–832.
- (21) Weller, L.; Thacker, V. V.; Herrmann, L. O.; Hemmig, E. A.; Lombardi, A.; Keyser, U. F.; Baumberg, J. J. Gap-Dependent Coupling of Ag-Au Nanoparticle Heterodimers Using DNA Origami-Based Self-Assembly. *ACS Photonics* **2016**, *3*, 1589–1595.

- (22) Woo, K. C.; Shao, L.; Chen, H. J.; Liang, Y.; Wang, J. F.; Lin, H. Q. Universal Scaling and Fano Resonance in the Plasmon Coupling between Gold Nanorods. *ACS Nano* **2011**, *5*, 5976–5986.
- (23) Slaughter, L. S.; Wu, Y. P.; Willingham, B. A.; Nordlander, P.; Link, S. Effects of Symmetry Breaking and Conductive Contact on the Plasmon Coupling in Gold Nanorod Dimers. *ACS Nano* **2010**, *4*, 4657–4666.
- (24) Osberg, K. D.; Harris, N.; Ozel, T.; Ku, J. C.; Schatz, G. C.; Mirkin, C. A. Systematic Study of Antibonding Modes in Gold Nanorod Dimers and Trimers. *Nano Lett.* **2014**, *14*, 6949–6954.
- (25) Malachosky, E. W.; Guyot-Sionnest, P. Gold Bipyramid Nanoparticle Dimers. *J. Phys. Chem. C* **2014**, *118*, 6405–6412.
- (26) Mukherjee, S.; Sobhani, H.; Lassiter, J. B.; Bardhan, R.; Nordlander, P.; Halas, N. J. Fano Resonances: Nanoparticles with Built-in Fano Resonances. *Nano Lett.* **2010**, *10*, 2694–2701.
- (27) Flauraud, V.; Bernasconi, G. D.; Butet, J.; Alexander, D. T. L.; Martin, O. J. F.; Braggar, J. Mode Coupling in Plasmonic Heterodimers Probed with Electron Energy Loss Spectroscopy. *ACS Nano* **2017**, *11*, 3485–3495.
- (28) Quillin, S. C.; Cherqui, C.; Montoni, N. P.; Li, G. L.; Camden, J. P.; Masiello, D. J. Imaging Plasmon Hybridization in Metal Nanoparticle Aggregates with Electron Energy-Loss Spectroscopy. *J. Phys. Chem. C* **2016**, *120*, 20852–20859.
- (29) Liu, M.; Lee, T.-W.; Gray, S. K.; Guyot-Sionnest, P.; Pelton, M. Excitation of dark plasmons in metal nanoparticles by a localized emitter. *Phys. Rev. Lett.* **2009**, *102*, No. 107401.
- (30) Fan, J. A.; Wu, C. H.; Bao, K.; Bao, J. M.; Bardhan, R.; Halas, N. J.; Manoharan, V. N.; Nordlander, P.; Shvets, G.; Capasso, F. Self-Assembled Plasmonic Nanoparticle Clusters. *Science* **2010**, *328*, 1135–1138.
- (31) Zhan, Q. W. Cylindrical vector beams: from mathematical concepts to applications. *Adv. Opt. Photonics* **2009**, *1*, 1–57.
- (32) Woźniak, P.; Banzer, P.; Leuchs, G. Selective switching of individual multipole resonances in single dielectric nanoparticles. *Laser Photonics Rev.* **2015**, *9*, 231–240.
- (33) Manna, U.; Lee, J. H.; Deng, T. S.; Parker, J.; Shepherd, N.; Weizmann, Y.; Scherer, N. F. Selective Induction of Optical Magnetism. *Nano Lett.* **2017**, *17*, 7196–7206.
- (34) Zuchner, T.; Failla, A. V.; Meixner, A. J. Light Microscopy with Doughnut Modes: A Concept to Detect, Characterize, and Manipulate Individual Nanoobjects. *Angew. Chem., Int. Ed.* **2011**, *50*, 5274–5293.
- (35) Bautista, G.; Kauranen, M. Vector-Field Nonlinear Microscopy of Nanostructures. *ACS Photonics* **2016**, *3*, 1351–1370.
- (36) Sancho-Parramon, J.; Bosch, S. Dark modes and Fano resonances in plasmonic clusters excited by cylindrical vector beams. *ACS Nano* **2012**, *6*, 8415–8423.
- (37) Yan, J. H.; Liu, P.; Lin, Z. Y.; Wang, H.; Chen, H. J.; Wang, C. X.; Yang, G. W. Magnetically induced forward scattering at visible wavelengths in silicon nanosphere oligomers. *Nat. Commun.* **2015**, *6*, No. 7042.
- (38) Das, T.; Iyer, P. P.; DeCrescent, R. A.; Schuller, J. A. Beam engineering for selective and enhanced coupling to multipolar resonances. *Phys. Rev. B* **2015**, *92*, No. 241110.
- (39) Das, T.; Schuller, J. A. Dark modes and field enhancements in dielectric dimers illuminated by cylindrical vector beams. *Phys. Rev. B* **2017**, *95*, No. 201111.
- (40) Gómez, D. E.; Teo, Z. Q.; Altissimo, M.; Davis, T. J.; Earl, S.; Roberts, A. The Dark Side of Plasmonics. *Nano Lett.* **2013**, *13*, 3722–3728.
- (41) Yanai, A.; Grajower, M.; Lerman, G. M.; Hentschel, M.; Giessen, H.; Levy, U. Near- and Far-Field Properties of Plasmonic Oligomers under Radially and Azimuthally Polarized Light Excitation. *ACS Nano* **2014**, *8*, 4969–4974.
- (42) Bao, Y.; Hu, Z. J.; Li, Z. W.; Zhu, X.; Fang, Z. Y. Magnetic Plasmonic Fano Resonance at Optical Frequency. *Small* **2015**, *11*, 2177–2181.
- (43) Albrecht, W.; Deng, T. S.; Goris, B.; van Huis, M. A.; Bals, S.; van Blaaderen, A. Single Particle Deformation and Analysis of Silica-Coated Gold Nanorods before and after Femtosecond Laser Pulse Excitation. *Nano Lett.* **2016**, *16*, 1818–1825.
- (44) Stalder, M.; Schadt, M. Linearly polarized light with axial symmetry generated by liquid-crystal polarization converters. *Opt. Lett.* **1996**, *21*, 1948–1950.
- (45) Taflove, A.; Hagness, S. C. *Computational Electrodynamics: The Finite-Difference Time-Domain method*, 3rd ed.; Artech House: Boston, London, 2004.
- (46) Oskooi, A. F.; Roundy, D.; Ibanescu, M.; Bermel, P.; Joannopoulos, J. D.; Johnson, S. G. MEEP: A flexible free-software package for electromagnetic simulations by the FDTD method. *Comput. Phys. Commun.* **2010**, *181*, 687–702.
- (47) Johnson, P. B.; Christy, R. W. Optical constants of noble metals. *Phys. Rev. B* **1972**, *6*, 4370–4379.
- (48) Grahn, P.; Shevchenko, A.; Kaivola, M. Electromagnetic multipole theory for optical nanomaterials. *New J. Phys.* **2012**, *14*, No. 093033.
- (49) Mühlig, S.; Menzel, C.; Rockstuhl, C.; Lederer, F. Multipole analysis of meta-atoms. *Metamaterials* **2011**, *5*, 64–73.
- (50) Parker, J.; Gray, S.; Scherer, N. F. Multipolar Analysis of Electric And Magnetic Modes Excited by Vector Beams in Core-satellite Nanostructures. 2017, arXiv preprint arXiv:1711.06833. arXiv.org e-Print archive. <https://arxiv.org/abs/1711.06833>.
- (51) Mie, G. Beirgrade zur optik truber medien, speziell kolloidaler metallosungen. *Ann. Phys.* **1908**, *330*, 377–455.
- (52) Jain, P. K.; Eustis, S.; El-Sayed, M. A. Plasmon coupling in nanorod assemblies: Optical absorption, discrete dipole approximation simulation, and exciton-coupling model. *J. Phys. Chem. B* **2006**, *110*, 18243–18253.
- (53) Dorn, R.; Quabis, S.; Leuchs, G. Sharper focus for a radially polarized light beam. *Phys. Rev. Lett.* **2003**, *91*, No. 233901.
- (54) Romero, I.; Aizpurua, J.; Bryant, G. W.; de Abajo, F. J. G. Plasmons in nearly touching metallic nanoparticles: singular response in the limit of touching dimers. *Opt. Express* **2006**, *14*, 9988–9999.
- (55) Atay, T.; Song, J. H.; Nurmikko, A. V. Strongly interacting plasmon nanoparticle pairs: From dipole-dipole interaction to conductively coupled regime. *Nano Lett.* **2004**, *4*, 1627–1631.
- (56) Youngworth, K.; Brown, T. G. Focusing of high numerical aperture cylindrical-vector beams. *Opt. Express* **2000**, *7*, 77–87.

Supporting Information

Dark Plasmon Modes in Symmetric Gold Nanoparticle Dimers Illuminated by Focused Cylindrical Vector Beams

Tian-Song Deng^{1,2,§}, John Parker^{2,3,§}, Yuval Yifat², Nolan Shepherd^{1,2}, Norbert F. Scherer^{1,2,*}

¹The James Franck Institute, ²Department of Chemistry, ³Department of Physics, University of Chicago, Chicago, USA

[§]These authors contributed equally to this work.

*Email: nfschere@uchicago.edu

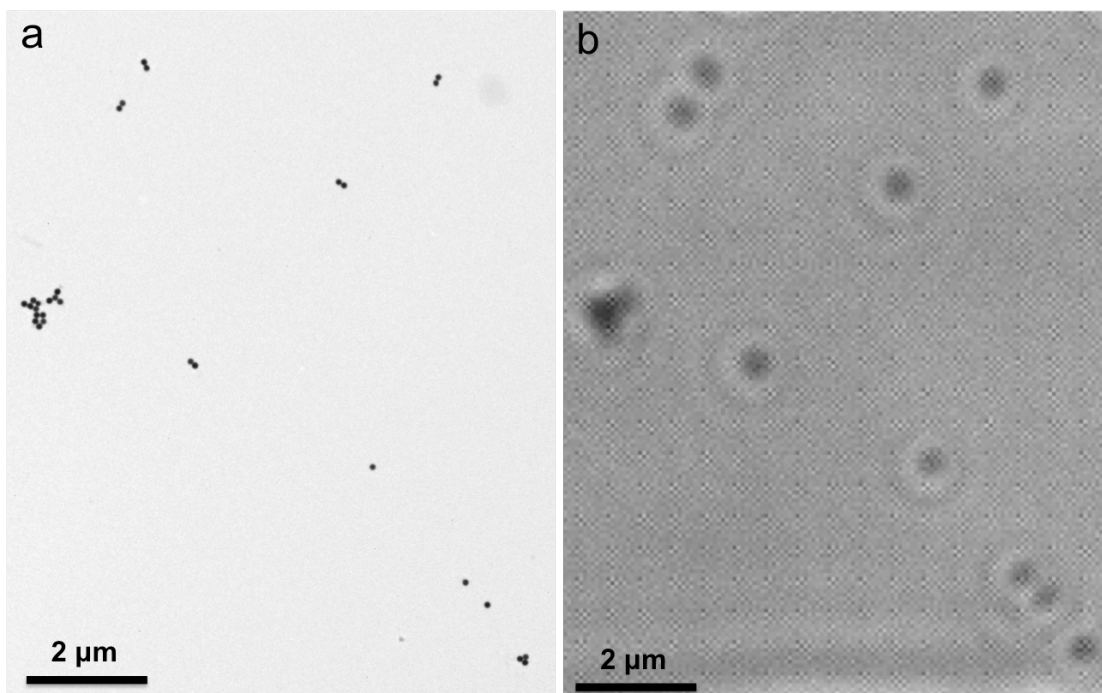


Figure S1. TEM (a) and optical microscope (b) images from the same area of the sample. We can readily conduct single particle spectroscopy measurements by using the EM finder grid. Their spatial correspondence and correlation allows obtaining the structure and scattering spectra of individual AuNP dimers. However, neither measurement is limited to dimer nanostructures. To avoid any possibility of scattering from neighbor particles that could affect the spectra measurement, the dimers we chose to measure are well separated ($\sim 5 \mu\text{m}$).

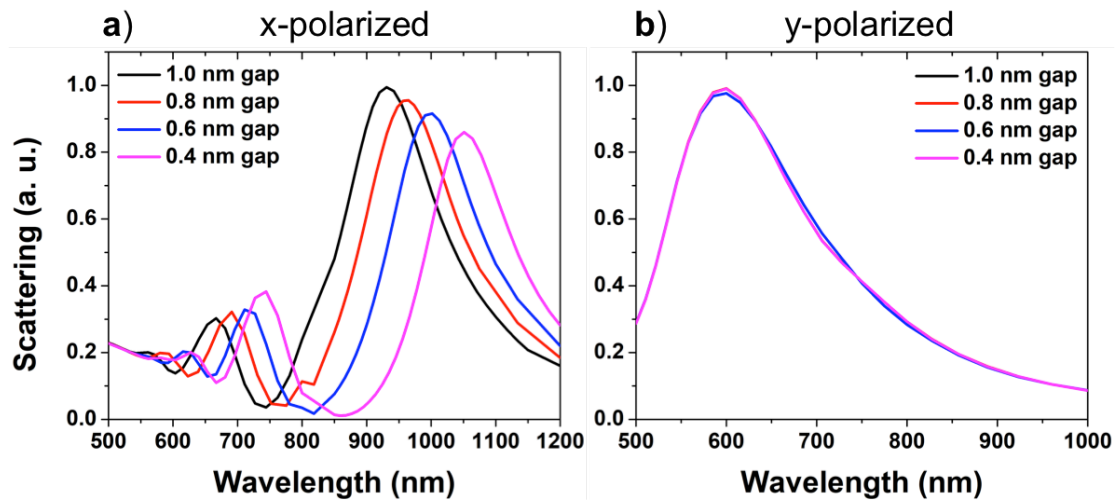


Figure S2. Simulated scattering spectra excited by linearly polarized beams. (a) The scattering spectra are obtained for polarization of the incident field parallel to the dimer axis (x-polarized), and (b) scattering spectra obtained for illuminating beams linearly polarized perpendicular to the dimer axis (y-polarized).

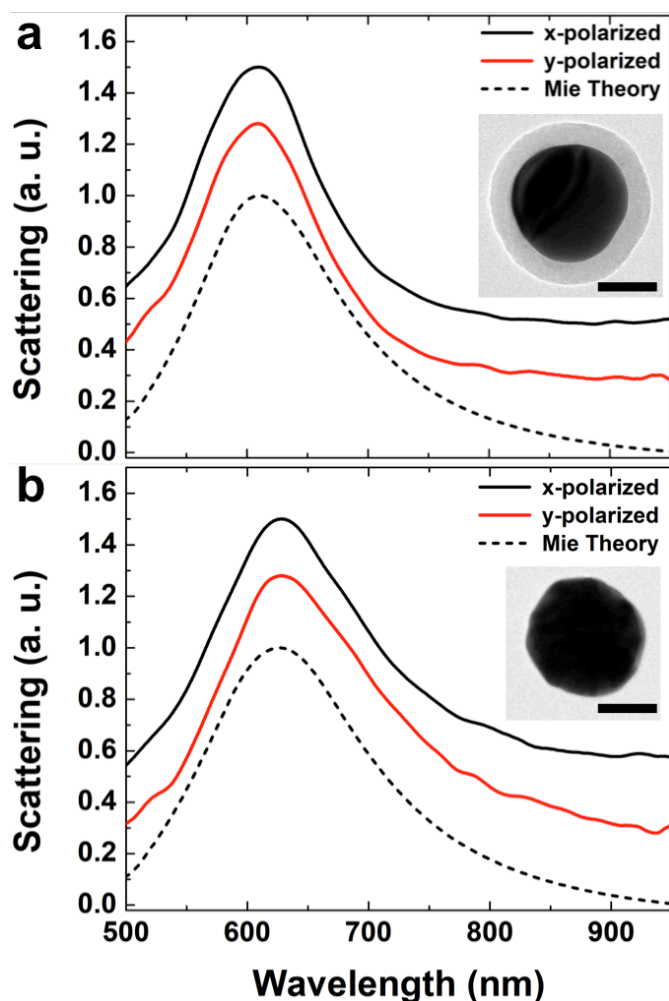


Figure S3. Scattering spectra of individual nanoparticles excited by a focused linearly polarized beam. (a) AuNP@SiO₂, the AuNP core is 105 nm in diameter, and the LSPR is peaked at 610 nm. (b) AuNP, 108 nm in diameter, and the LSPR is at 628 nm. Black solid curves are the scattering spectra excited by light polarized along the x-axis direction. Red solid curves are the spectra excited by y-polarized light. Black dashed curves are the scattering spectra calculated by Mie theory. The Mie scattering spectra were calculated using the values of particle size and SiO₂ shell thickness measured from TEM images. The effective refractive index n of the environment used for Au@SiO₂ is 1.47 (between SiO₂ ($n = 1.45$) and immersion oil ($n = 1.51$)), and for AuNP is 1.51 (refractive index of immersion oil). TEM images in the insets are the same nanoparticles that gave rise to the scattering spectra obtained with focused linearly polarized optical beams. The scale bars in the TEM images are 50 nm.

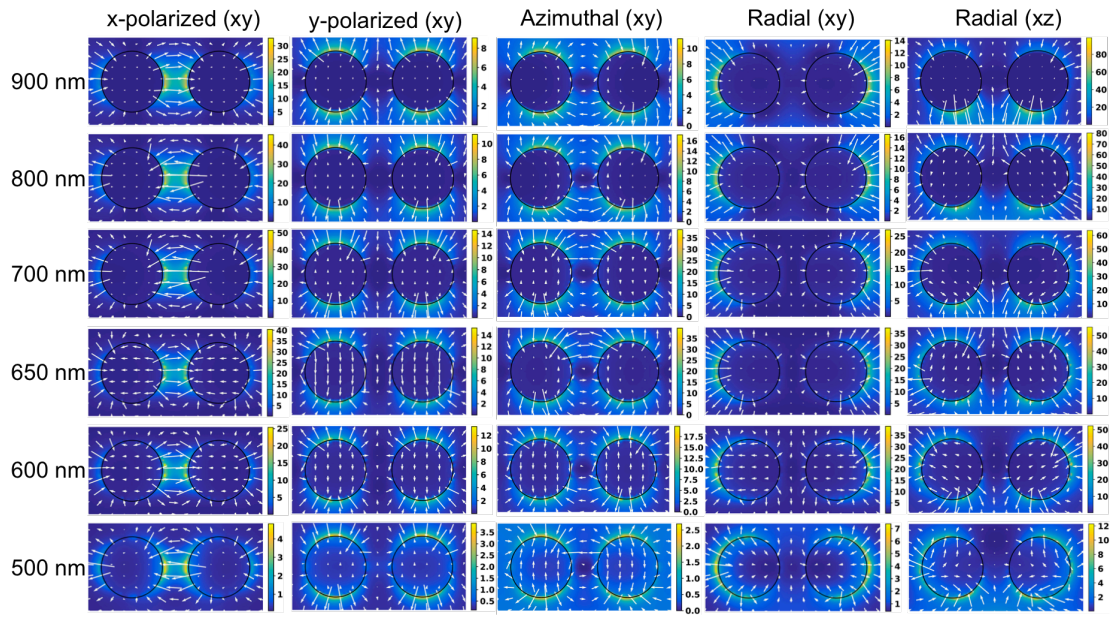


Figure S4. Near field intensity distribution for x-polarized, y-polarized, azimuthally and radially polarized light. The simulated AuNP diameter is 100 nm with 40 nm gap distance. The 1st to 4th columns are the xy plane (focal plane) and the 5th column is the xz plane. Six wavelengths of 900 nm, 800 nm, 700 nm, 650 nm, 600 nm, and 500 nm were selected for each polarization.

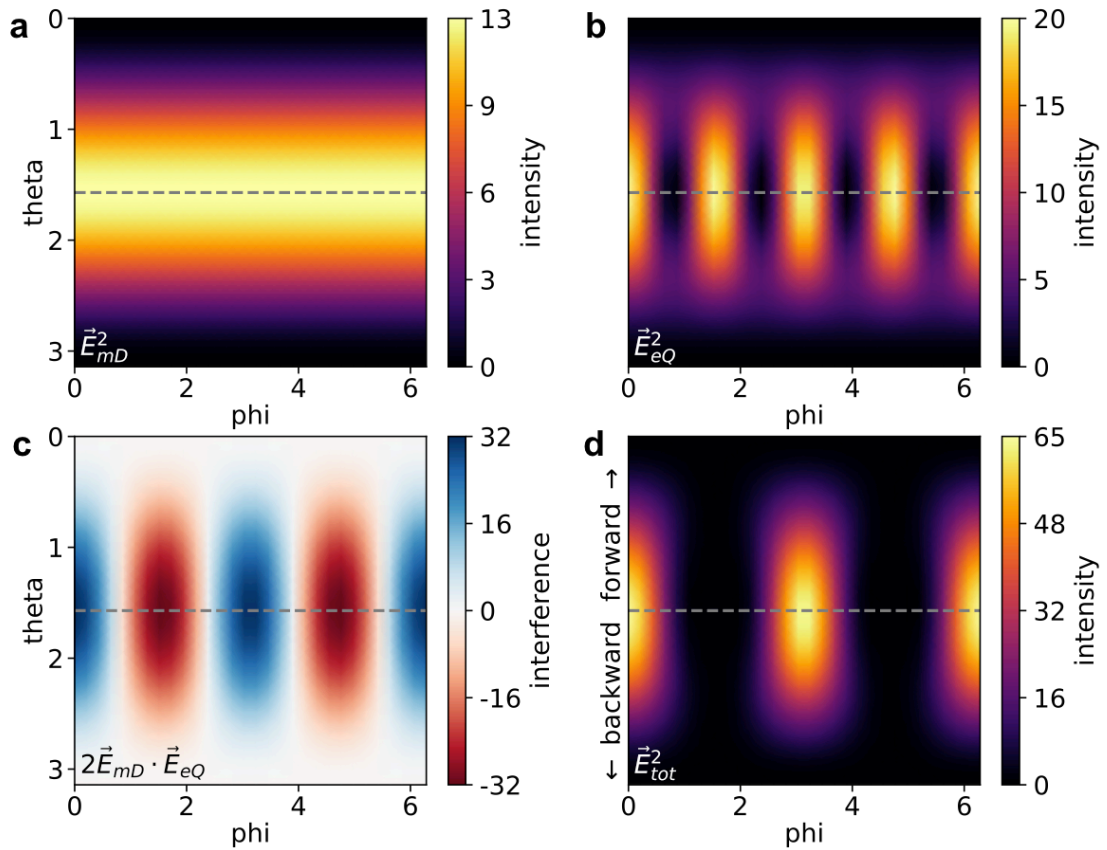


Figure S5. Angular scattering distributions obtained from FDTD simulations of the AuNP dimer (with 40 nm gap) for azimuthally polarized beam illumination. (a) Angular scattering of the z-oriented magnetic dipole mode. **(b)** Angular scattering of the electric quadrupole mode. **(c)** Angular scattering of the interference term between magnetic dipole and electric quadrupole modes. Red denotes destructive interference and blue denotes constructive interference. **(d)** Total angular scattering of the AuNP dimer. The interference between the magnetic dipole and electric quadrupole modes creates an interference pattern of similar intensity both in the forward and backward direction.

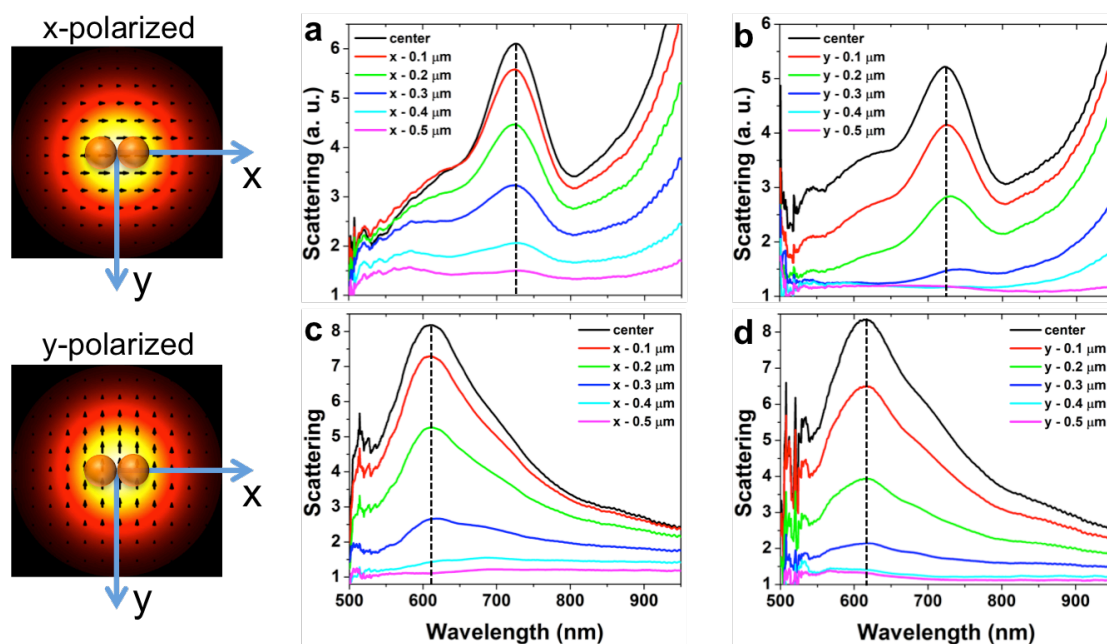


Figure S6. AuNP dimer (sub-nanometer gap) spectra at different x- and y-positions with respect to the beam axis. (a)-(b) Scattering spectra for x-polarized beam (parallel to the dimer axis) while moving the AuNP dimer in the x- (a) and y- (b) directions. (c)-(d) Scattering spectra for y-polarized beam (perpendicular to the dimer axis) while repositioning the AuNP dimer along the x- (c) and y- (d) directions. The left panels schematically indicate the directions of the spatial shifts along the x- and y-directions. The black curves in (a)-(d) are the spectra obtained when the AuNP dimer is centered on the optical beam axis. The black dashed lines indicate the plasmon resonance peak wavelengths, which don't change while spatially shifting the AuNP dimer away from the center of the incident beam. The particle and beam size shown in the left panels are from the simulation indicating their spatial overlap.

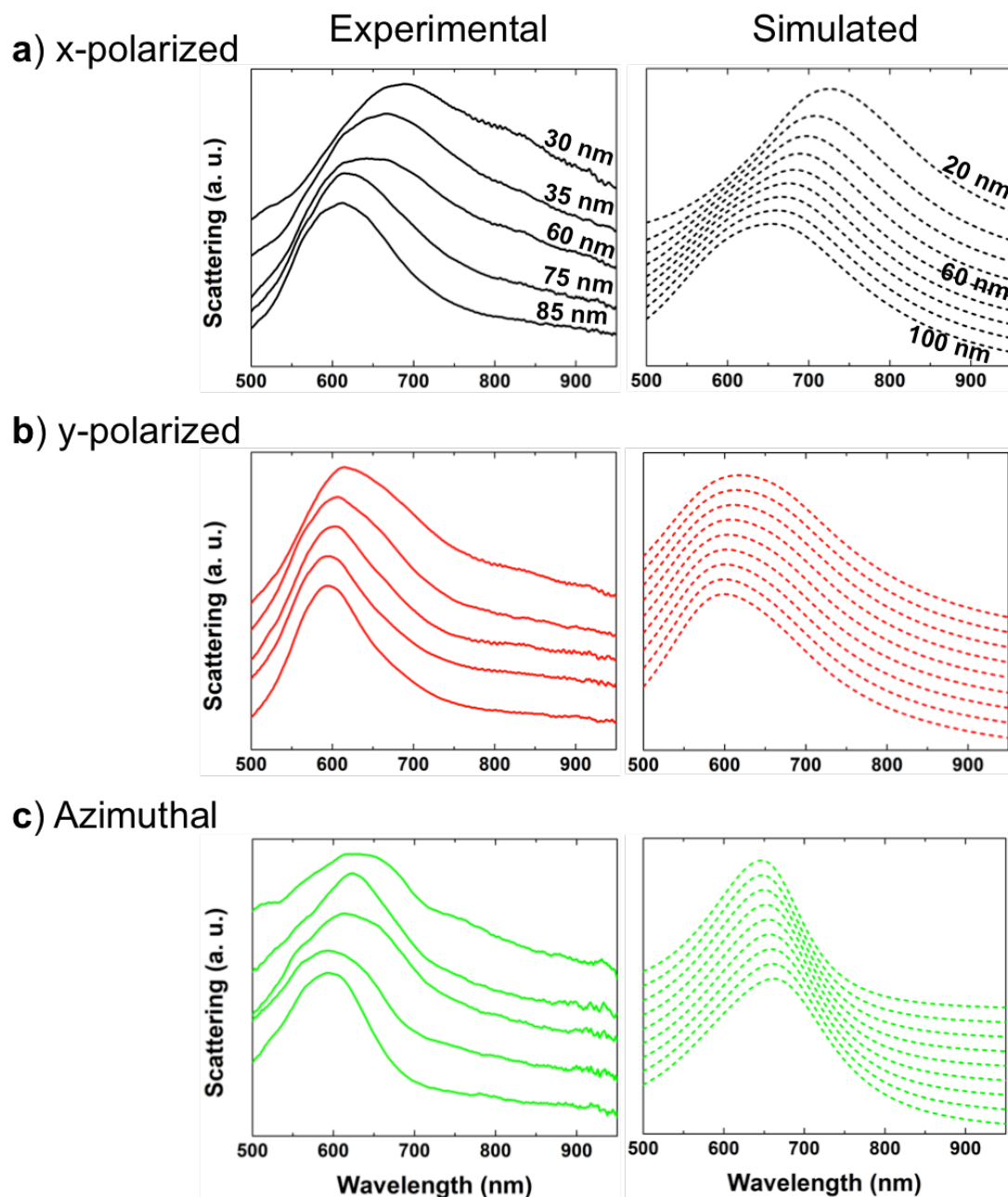


Figure S7. Experimental and simulated spectra of AuNP dimers with different gaps excited by (a) x-polarized, (b) y-polarized, and (c) azimuthally polarized light. From top to bottom, the gaps are 30 nm, 35 nm, 60 nm, 75 nm, and 85 nm in the experimental spectra, and are from 20 to 100 nm, with step size of 10 nm in the simulated spectra. The experimental and simulated spectra are in good agreement.

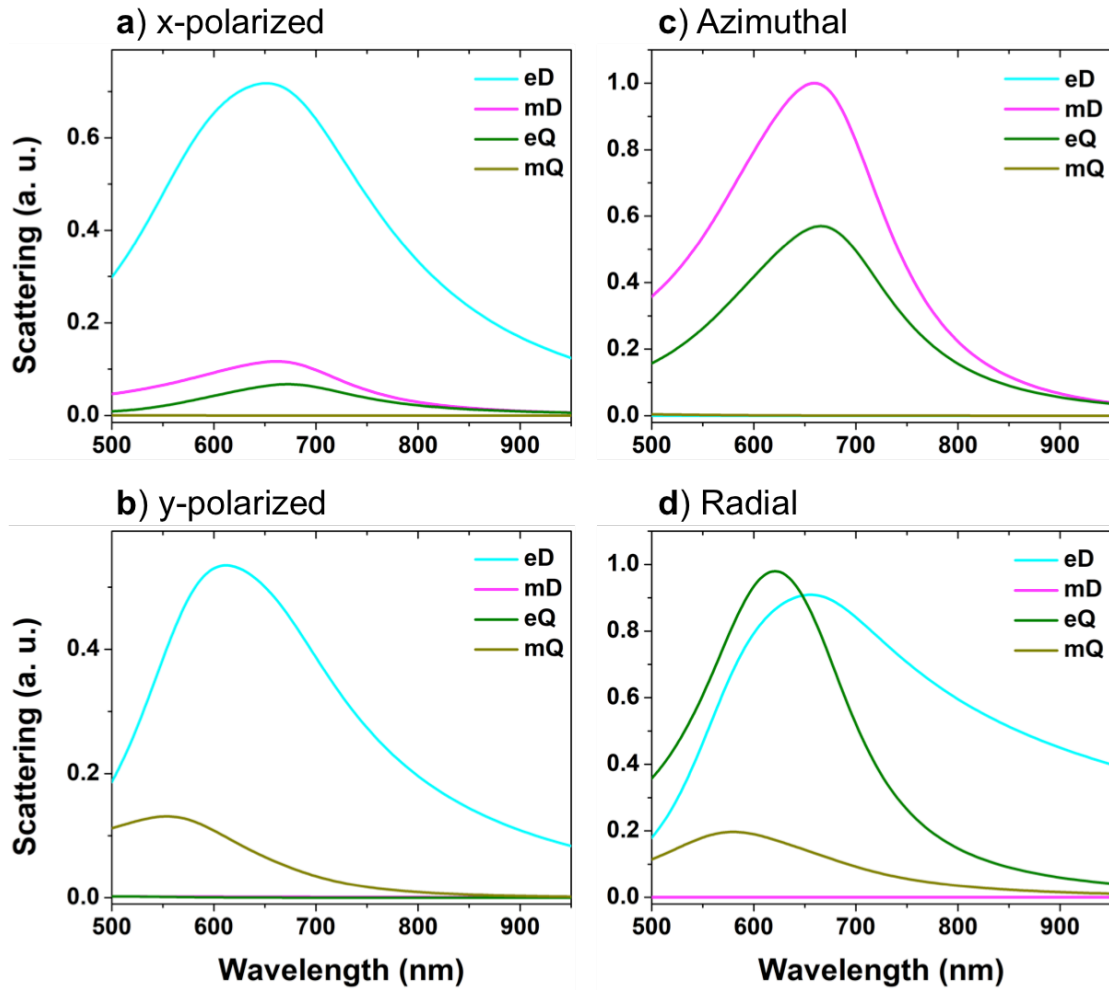
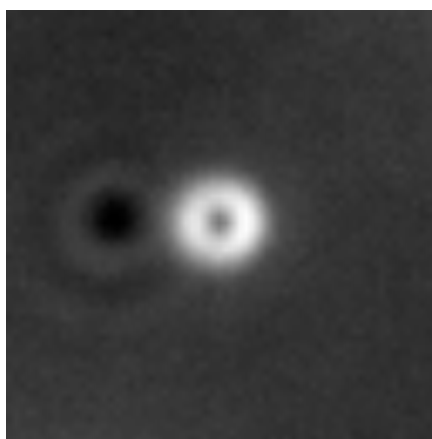


Figure S8. Expansion of the FDTD scattering amplitudes into electric and magnetic multipolar modes for a 100 nm gap AuNP dimer. The simulated results are for (a) x-polarized, (b) y-polarized, (c) azimuthally polarized, and (d) radially polarized beam excitation. Compared to the 40 nm gap AuNP dimer (Figure 3d), the scattering spectra associated with the eD and eQ modes are more overlapped for radial beam illumination, resulting in more symmetric spectra (Figure 7c, bottom spectra).



Video S1. The AuNP dimer shifted from left side to the right side of the doughnut shaped vector beams with 200 nm step size. During the shift, the AuNP dimer is from left side, left arc, center, right arc, and right side of the vector beams.